JACS
JOURNAL OF THE AMERICAN CHEMICAL SOCIETY

Article

pubs.acs.org/JACS

Giant Electroactive M_4L_6 Tetrahedral Host Self-Assembled with Fe(II) Vertices and Perylene Bisimide Dye Edges

Kingsuk Mahata, Peter D. Frischmann, and Frank Würthner*

Institut für Organische Chemie and Center for Nanosystems Chemistry, Universität Würzburg, Am Hubland, 97074 Würzburg, Germany

Supporting Information

ABSTRACT: Self-assembly of octahedral Fe(II) ions and linear perylene bisimide (PBI) dyes with 2,2′-bipyridine groups covalently attached at the imide positions quantitatively yields an $Fe_4(PBI)_6$ tetrahedron by the directional bonding approach. With an edge length of 3.9 nm and estimated internal volume >950 Å^3, tetrahedron **T** is one of the largest M_4L_6 tetrahedra ever reported. Importantly, many of the desirable photo- and electroactive properties of the PBI ligands are transferred to the nanoscale metallosupramolecule. Tetrahedron **T** absorbs strongly across the visible spectrum out to 650 nm and exhibits a total of 7 highly reversible electrochemical oxidation and reduction waves spanning a 3.0 V range. This facile cycling of 34 electrons between +18 and −16 charged species is likely enabled due to the porous nature of the tetrahedron that allows the necessary counterions to freely flow in and out of the host. Host−guest encapsulation of C_{60} by **T** in acetonitrile was studied by ^{13}C NMR spectroscopy, UV−vis spectroscopy, and ESI-MS, confirming that the tetrahedron is a suitable host for large, functional guest molecules.

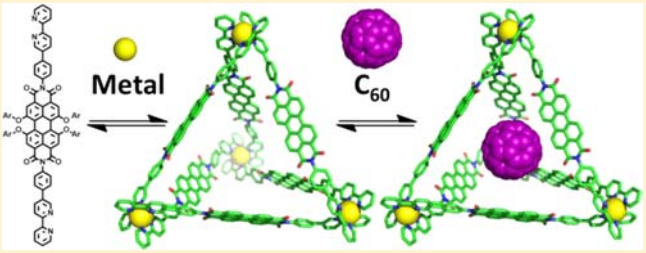

INTRODUCTION

Since the discovery of crown ethers, cryptands, and cavitands, the field of host−guest chemistry has developed dramatically. While the initial focus was on the encapsulation of small molecules or ions, recent research efforts have shifted to designing larger hosts that are capable of encapsulating inorganic catalysts, larger substrates, and even small peptide sequences.[1] To access hosts with sufficiently large dimensions, a metal coordination directed self-assembly strategy is often applied, where the geometry of the ligands combined with the metal coordination number and geometry determine the reaction outcome.[2] Using this strategy, large and often high-symmetry metallosupramolecular hosts may be isolated in near quantitative yields. Much like enzymes, synthetic hosts bind suitable guest molecules based on size and complementary interactions, and reactions occurring inside synthetic hosts can exhibit substrate selectivity, rate enhancements, and unusual regioselectivity.[3]

A rising interest in reactions driven by photoinduced electron transfer (PET), in particular, for the production of solar fuels,[4] presents opportunities to design new hosts that absorb visible light and exhibit favorable redox chemistry for photosensitization. Although most synthetic hosts are transparent to visible light and are redox-inactive or exhibit irreversible redox waves in catalytically relevant ranges, some fascinating examples of host−guest PET exist. Photosensitized oxidation of encapsulated adamantane to 1-adamantanol within a Pd_6L_4 tris-pyridyltriazine-based host was demonstrated by Fujita and co-workers.[5] Using the same host, photodriven anti-Markovnikov hydration of internal alkynes was also reported.[6] In each example, the photoexcited triazine units accept an electron from the encapsulated guest; however, the critical PET is only responsive to UV light. Similarly, UV-light-sensitized PET was reported by Ramamurthy and co-workers from anionic deep cavity resorcinarene-based cavitands to cationic acceptors electrostatically bound to the surface of the hosts.[7] Moving into the visible spectrum, Sallé and co-workers recently reported two electroactive metallosupramolecular hosts self-assembled with tetrathiafulvalenepyridyl-based ligands that bind electron-poor guests and show spontaneous electron transfer to encapsulated tetrafluorotetracyano-*p*-quinodimethane.[8] Duan and co-workers successfully demonstrated host−guest photosensitized H_2 evolution from a diiron hydrogenase mimic encapsulated within a carbazole-based metallosupramolecular basket.[9] Synthetic hosts may also regulate electron- and energy-transfer behavior between encapsulated guests and acceptors in solution.[10]

To contribute to this underdeveloped but promising area of host−guest photo- and electrochemistry, we describe here our initial efforts toward integrating visible-light photofunctional and redox-active perylene bisimide (PBI) ligands into large metallosupramolecular hosts. PBI dyes show outstanding photophysical and electrochemical properties and have been used to construct various metallosupramolecular macrocycles.[11] Many of these supramolecules exhibit desirable photophysics

Received: August 19, 2013
Published: September 23, 2013

   dx.doi.org/10.1021/ja4083039 | J. Am. Chem. Soc. 2013, 135, 15656−15661

such as wide-range visible-light absorption, long-lived excited states,[12] and directional excitation energy transfer resulting in sensitized emission.[11c] Despite their superb photophysical properties and central cavity, none of the PBI-based metallomacrocycles showed affinity for guest encapsulation. In addition, owing to weak monodentate metal−pyridyl bonding, such macrocycles dissociate under highly dilute conditions or in polar solvents and are prone to reorganization into metallosupramolecular polymers at high concentration.[13] This led us to tune our strategy to fabricate more robust three-dimensional metallosupramolecular hosts with PBI-derived ligands. Lindoy, Meehan, and co-workers reported that the coordination of octahedral metal ions, such as Fe^{2+}, by linearly arranged bis-bipyridine ligands yields metallosupramolecular tetrahedra that are capable of encapsulating guest molecules in their internal void space.[14] Combining this strategy with our experience in synthesizing PBI-based metallosupramolecules led us to design ligand **L** that successfully organizes into a very large, visible-light absorbing, and electroactive tetrahedral host **T** as shown in Scheme 1.

EXPERIMENTAL SECTION

General. High-resolution mass spectra (ESI) were recorded on an ESI micrOTOF Focus from Bruker Daltonics. UV−vis absorption spectra were measured either on a Perkin-Elmer Lambda 35 or on a Perkin-Elmer Lambda 40 spectrophotometer. Temperature was controlled by a PTP-1 Peltier element (Perkin-Elmer). Cyclic voltammetry experiments were carried out using a BAS Cell Stand C3, BAS Epsilon with *n*-Bu_4NPF_6 (0.1 M) as electrolyte against a Ag/AgCl reference electrode, Pt wire as auxiliary electrode, 1 mm Pt disk as working electrode, and ferrocene as internal standard. ^{1}H NMR spectra were recorded either on a Bruker Avance 400 or Bruker Avance DMX 600 MHz spectrometer at 293 K unless otherwise stated. The viscosity of the 1:1 $CD_3CN/CDCl_3$ solution used in the Stokes−Einstein equation to analyze the ^{1}H DOSY NMR spectrum of $\mathbf{T_1}$ was taken as 0.478 mPa from Lazarte et al.[15] Fullerene C_{60} was obtained from MTR Ltd. (99.5%).

Synthesis of T_1 and T_2. Under an inert atmosphere, compound **L** (6 equiv) and $[Fe(H_2O)_6]X_2$ (4 equiv) were combined in a Schlenk tube. After addition of nitrogen-purged acetonitrile (10 mL) and chloroform (10 mL), the mixture was stirred at 70 °C for 12 h. Solvents were evaporated, and the residue was washed with water (50 mL). The product was isolated quantitatively.

Fullerene Encapsulation. In a typical procedure, metallosupramolecular tetrahedra (c = 0.5−1.0 × 10^{-3} M) were stirred in the presence of a large excess of fullerene (10 equiv; calculated from C_{60} content) in a mixture of $CH_3CN/CHCl_3$ (9:1) overnight at 70 °C. The solvents were removed under reduced pressure, and the residue was suspended in CH_3CN. Excess C_{60} was removed by filtration (VWR International 13 mm syringe filter with 0.45 μm PTFE membrane). The filtrate was evaporated, suspended in $CHCl_3$, sonicated, and filtered, washing away any remaining unbound C_{60} left in the first filtrate. The precipitate was redissolved in CH_3CN to yield a solution of the host−guest complex that was analyzed without further purification.

Scheme 1. Self-Assembly of T_1 ($[Fe_4L_6](BF_4)_8$) and T_2 ($[Fe_4L_6](OTf)_8$) from L[a]

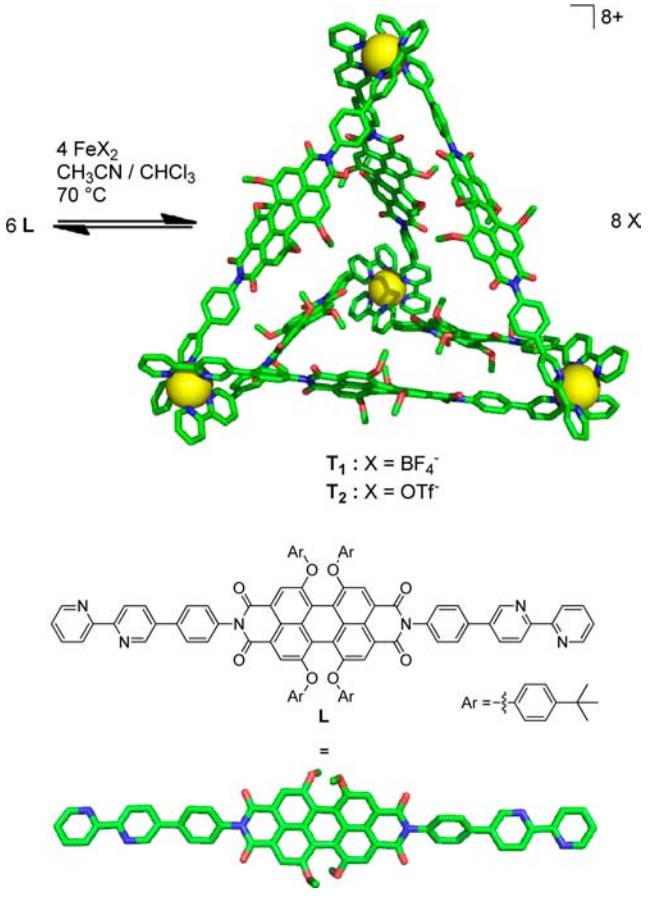

[a]The tetrahedron model is depicted with all $Fe(bpy)_3$ vertices in the Δ conformation. Hydrogen atoms are omitted, and OPh^{t}Bu bay substituents are represented as OMe for clarity (C = green, N = blue, O = red, Fe = yellow).

RESULTS AND DISCUSSION

Synthesis and Characterization. Bipyridine containing bis-bidentate ligand **L** was targeted to fabricate metallosupramolecular M_4L_6 tetrahedra (Scheme 1). Synthesis of the ligand was straightforward and achieved in good yield (88%) via imidization of 1,6,7,12-tetra(4-*tert*-butylphenoxy)perylene-3,4:9,10-tetracarboxylic acid bisanhydride[11a] with 5-(4-aminophenyl)-2,2′-bipyridine. Reacting **L** with FeX_2 (X = BF_4, OTf) in a mixture of $CH_3CN/CHCl_3$ (1:1) for 12 h at 70 °C under a nitrogen atmosphere yielded metallosupramolecular tetrahedra $\mathbf{T}_n$ (n = 1, X = BF_4; n = 2, X = OTf). The structure and physical properties of $\mathbf{T_1}$ and $\mathbf{T_2}$ were established using a combination of high-resolution mass spectrometry, ^{1}H NMR and diffusion-ordered spectroscopy (DOSY), UV−vis spectroscopy, and cyclic voltammetry (CV).

A typical electrospray ionization time-of-flight (ESI-TOF) mass spectrum of $\mathbf{T_1}$ = $[Fe_4L_6](BF_4)_8$ is depicted in Figure 1a and shows four peaks that are exclusively associated with the metallosupramolecular tetrahedron. The most abundant peak was observed at m/z = 1110.661 that shows the characteristic m/z splitting for a 8+ charged species of 0.125 mass units and was assigned to $[Fe_4L_6]^{8+}$. Three less abundant peaks, corresponding to tetrahedron−counterion complexes, were noticed at m/z = 1281.756, 1509.718, and 1829.065 and assigned to $[Fe_4L_6](BF_4)^{7+}$, $[Fe_4L_6](BF_4)_2^{6+}$, and $[Fe_4L_6](BF_4)_3^{5+}$, respectively. A similar mass spectrum was obtained for $\mathbf{T_2}$ = $[Fe_4L_6](OTf)_8$ that exclusively shows peaks that correspond to the tetrahedral assembly (Supporting Information Figure S12).

Resonances in the ^{1}H NMR spectra of the metallosupramolecular assemblies $\mathbf{T_1}$ and $\mathbf{T_2}$ were broad (Supporting Information Figure S4) due to the presence of many diastereomers arising from the chirality of the four octahedral metal complexes and the chirality of each of the core-twisted

dx.doi.org/10.1021/ja4083039 | J. Am. Chem. Soc. 2013, 135, 15656−15661

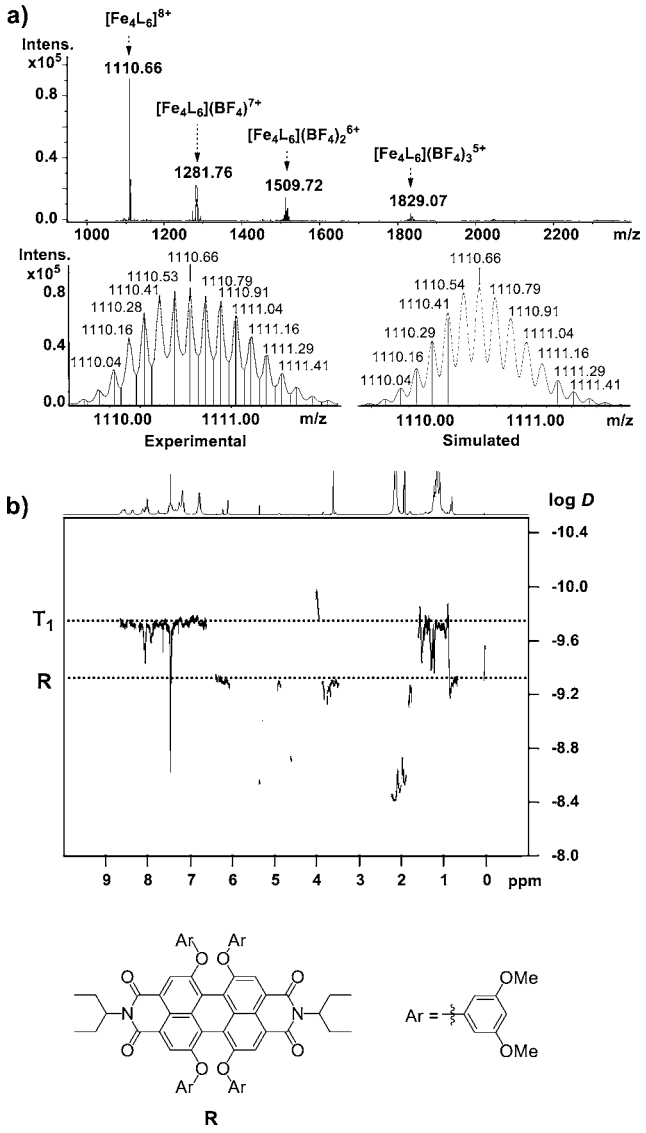

Figure 1. (a) ESI-TOF mass spectrum of $\mathbf{T_1}$ in CH_3CN along with the experimental (bottom left) and simulated (bottom right) isotopic distributions for $[Fe_4L_6]^{8+}$. (b) ^1H DOSY NMR spectrum of $\mathbf{T_1}$ and reference PBI **R** in a 1:1 $CD_3CN/CDCl_3$ mixture.

PBI ligands (*P*- and *M*-atropisomers).[16] Such diastereoisomerism is known for metallosupramolecular tetrahedra.[17] In search of more evidence for discrete tetrahedron self-assembly, we performed a ^1H DOSY NMR experiment with $\mathbf{T_1}$, as the technique has previously been applied to establish the size and structure of metallosupramolecular assemblies in solution.[18] The ^1H DOSY spectrum of $\mathbf{T_1}$ (Figure 1b) was carried out in the presence of reference PBI **R**, chosen for its reasonable solubility in $CD_3CN/CDCl_3$ mixtures (see Figure 1, bottom, for the structure of **R**). Diffusion coefficients were calculated for $\mathbf{T_1}$ (1.96×10^{-10} m^2 s^{-1} at 8.56 ppm) and **R** (5.16×10^{-10} m^2 s^{-1} at 6.11 ppm) by fitting the dependence of the signal intensities to the magnetic field gradient strength (Supporting Information Figure S8). The Stokes–Einstein equation, $D = k_BT/6\pi\eta r_s$, where D is the diffusion coefficient for a spherical assembly, was then applied to calculate the hydrodynamic radii of $\mathbf{T_1}$ and **R**. Experimental radii of 2.29 and 0.87 nm were determined for $\mathbf{T_1}$ and **R**, respectively, in close agreement with values obtained from molecular modeling (1.90 and 0.80 nm for $\mathbf{T_1}$ and **R**, respectively). Additionally, the single diffusion coefficient observed for all resonances associated with $\mathbf{T_1}$ further supports the exclusive formation of a metallosupramolecular tetrahedron.

UV–Vis Spectroscopy. To quantify the visible-light absorption of the self-assembled tetrahedral host, the photophysical behavior of **L**, $\mathbf{T_1}$, and $\mathbf{T_2}$ was investigated by UV–vis spectroscopy, and the spectra are depicted in Figure 2.

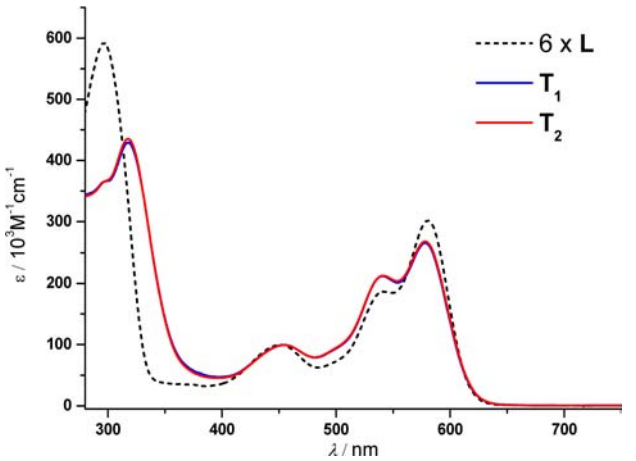

Figure 2. UV–vis absorption spectra of **L** (intensity multiplied by six for comparison, black dashed line), $\mathbf{T_1}$ (blue solid line), and $\mathbf{T_2}$ (red solid line). The spectra of $\mathbf{T_1}$ and $\mathbf{T_2}$ are identical. All spectra are recorded in a 1:1 $CH_3CN/CHCl_3$ mixture.

Tetrahedra $\mathbf{T_1}$ and $\mathbf{T_2}$ are most soluble in acetonitrile, and **L** is most soluble in chloroform; therefore, all measurements were conducted in a 1:1 mixture of $CHCl_3/CH_3CN$ for comparative purposes. Absorption maxima of **L** are found at 297 nm (λ_{max1}), 542 nm (λ_{max2}), and 580 nm (λ_{max3}), and similar maxima are found at 317, 541, and at 578 nm for $\mathbf{T_1}$. The extinction coefficients of the assembly $\mathbf{T_1}$ at λ_{max1-3} are 435 300, 212 700, and 268 500 M^{-1} cm^{-1}, respectively, roughly equivalent to the summation of six PBI **L** ligands.

The spectral features of **L** are similar to other PBI-based ligands,[11c] except that **L** has a slightly higher molar absorptivity at 297 nm due to the $\pi \rightarrow \pi^*$ transition of the bipyridine units. Maxima at 542 and 580 nm are associated with $0 \rightarrow 1$ and $0 \rightarrow 0$ vibronic transitions, respectively. Upon metal coordination, the high-energy maximum bathochromically shifted around 20 nm, concurrent with a decrease in optical density. The relative intensities of the 580 and 542 nm bands also changed upon tetrahedron assembly. For the free ligand **L**, the $\varepsilon_{max3}/\varepsilon_{max2}$ ratio was calculated to be 1.62, whereas for $\mathbf{T_1}$ and $\mathbf{T_2}$, the value was 1.26. This shift may be rationalized by the contribution from the metal-to-ligand charge-transfer transition of the assembled $[Fe(bpy)_3]^{2+}$ complexes (bpy = 2,2′-bipyridine), which appear at 525 nm for the isolated complex,[19,20] resulting in an increase in the intensity of ε_{max2}. This observation also supports the presence of $[Fe(bpy)_3]^{2+}$ units in $\mathbf{T_1}$ and $\mathbf{T_2}$.

Although **L** exhibits strong fluorescence comparable to typical bay-substituted PBI dyes, after the introduction of Fe^{2+}, the fluorescence of the tetrahedron is negligible. Details regarding the mechanism of fluorescence quenching are under further investigation.

Cyclic Voltammetry. Both PBI and $[Fe(bpy)_3]^{2+}$ are known to undergo reversible and well-defined electrochemical oxidation and reduction processes. To probe the effects of

dx.doi.org/10.1021/ja4083039 | J. Am. Chem. Soc. 2013, 135, 15656–15661

Table 1. Redox Properties of L, $[Fe(bpy)_3](OTf)_2$, T_1, and T_2 (in V vs Fc/Fc^+)[a]

compounds	E_{ox} (PBI/PBI$^+$)	E_{ox} (Fe^{2+}/Fe^{3+})	E_{red} (PBI/PBI$^-$)	E_{red} (PBI$^-$/PBI^{2-})	E_{red} (bpy/bpy$^-$)	E_{red} (bpy/bpy$^-$)	E_{red} (bpy/bpy$^-$)
L	0.90		−1.17	−1.33			
$[Fe(bpy)_3](OTf)_2$		0.67			−1.74	−1.93	−2.17
T_1	0.95	0.73	−0.94	−1.11	−1.65	−1.84	−2.08
T_2	0.95	0.73	−0.94	−1.11	−1.66	−1.85	−2.09

[a]All measurements were performed in dry CH_3CN except for **L** (CH_2Cl_2) with 0.1 M n-Bu_4NPF_6 as electrolyte.

tetrahedron assembly on the redox chemistry of the constituents, CV was performed on **L**, T_1, T_2, and model complex $[Fe(bpy)_3](OTf)_2$. Ligand **L** exhibits two reversible reductions and one reversible oxidation originating from the PBI unit, akin to other tetraphenoxy-substituted PBI derivatives (Supporting Information Figure S16).[11a] Reduction of the uncoordinated bipyridine units was not observed in the solvent window as the reduction potential of bipyridine is too low ($E_{1/2}$(bpy) = −2.10 V vs SCE).[21]

To assign the various redox processes associated with T_1 and T_2, we compared the voltammograms with electrochemical data of **L** and $[Fe(bpy)_3]^{2+}$. The redox potentials of $[Fe(bpy)_3]^{2+}$, **L**, T_1, and T_2 are summarized in Table 1. Reduction of the bpy units in $[Fe(bpy)_3]^{2+}$ is not simultaneous, and three successive bpy → bpy$^-$ reduction processes were previously reported by Braterman et al. (−1.54, −1.72, and −1.90 V vs Fc/Fc^+ in DMF).[20] We observed a similar scenario for $[Fe(bpy)_3](OTf)_2$ in acetonitrile (Supporting Information Figure S15). Two reversible oxidations along with five reversible reduction processes are observed for T_1 and T_2 (Figure 3 and Supporting

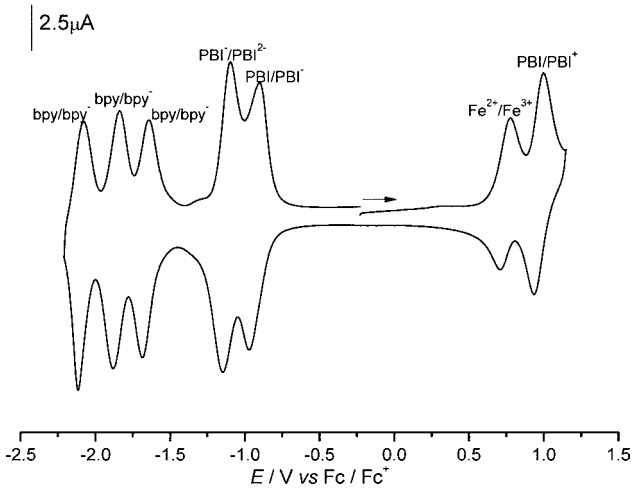

Figure 3. Cyclic voltammogram of T_1 in CH_3CN in the presence of 0.1 M n-Bu_4NPF_6 as supporting electrolyte (scan rate 200 mV s^{-1}). The values are given with regard to Fc/Fc^+, which has been used as internal standard for calibration of the Ag/AgCl reference electrode.

Information Figures S17 and S18). The first oxidation is associated with Fe^{2+} → Fe^{3+}, while the oxidation at higher potential is assigned to the process PBI → PBI$^+$. We attribute the slightly more difficult oxidation of Fe^{2+} in the tetrahedra to the proximity of the electron-deficient PBI units. Initial reductions of the metallosupramolecular tetrahedra (−0.94 and −1.11 V) are PBI centered and are due to successive reductions of PBI (PBI → PBI$^-$ → PBI^{2-}). Reductions found beyond −1.11 V are associated with the bipyridine units.

While the effect of self-assembly on the oxidation waves is minimal, the reduction processes are found to be more favorable for the tetrahedra than for the model compound $Fe[(bpy)_3]^{2+}$ (Table 1). This observation suggests that there is some electronic communication between the ligands and metal ions in the tetrahedra. The strong electron affinity of multiple PBI units organized in close proximity is likely responsible for the easier reductions. It is quite incredible that these metallosupramolecular tetrahedra may reversibly cycle between highly negative (16−) and positive (18+) species, representing a 34 electron swing, without significantly disturbing the integrity of the self-assembled tetrahedral framework. The highly porous structure of T_1 and T_2 may account for the reversibility because the cavity provides sufficient space to accommodate the necessary counterions, like an electrostatic sponge.

Molecular Modeling and C_{60} Host−Guest Encapsulation. All efforts to grow single crystals of T_n for an X-ray diffraction study were unsuccessful, likely due to the existence of many diastereomers. Therefore, to get a rough picture of the tetrahedron, a molecular force field MMFF geometry optimization was performed starting from the all-Δ diastereomer using the Spartan'08 software suite (Scheme 1 and Supporting Information Figure S20).[22] The energy-minimized all-Δ diastereomer exhibits a 3.9 nm edge (end to end distance of **L**), Fe^{2+}−Fe^{2+} distances of 2.9 nm, and apertures on the tetrahedral faces as large as 1.0 nm in diameter. The average distances between neighboring and opposing PBI cores are 1.5 and 2.1 nm, respectively (measured from the PBI centroids).

In solution, the PBI bay substituents are dynamic and may adopt many different conformations. Freely rotating bay substituents may act as aperture gates, affecting guest encapsulation and tuning the internal void space of the tetrahedra. Depending on the orientation of the OPh^{t}Bu bay substituents, the internal volume is conservatively estimated to be between 950 and 2150 Å^3, making these tetrahedra some of the largest in the M_4L_6 family.[23] Accordingly, these tetrahedra should be suited for the encapsulation of large functional guest molecules.

To prove this feature of T_n, our initial studies were directed toward the encapsulation of C_{60},[24] which is known to communicate electronically with PBI.[25] In a typical experiment, tetrahedra were treated with a large excess of C_{60} (10 equiv) and heated at 70 °C in a $CH_3CN/CHCl_3$ mixture (9:1) overnight. After removal of the solvents, the mixture was redissolved in CH_3CN and filtered to remove excess C_{60}, which is virtually insoluble in CH_3CN.[26] The host−guest assemblies were characterized by high-resolution mass spectrometry (ESI-TOF), ^{13}C NMR, and UV−vis spectroscopy. An ESI-TOF spectrum of T_1 and C_{60} is depicted in Figure 4a and shows prominent peaks at m/z = 1200.799 and 1290.801, which correspond to $[Fe_4L_6{\cdot}C_{60}]^{8+}$ and $[Fe_4L_6{\cdot}2C_{60}]^{8+}$, respectively. Free host $[Fe_4L_6]^{8+}$ was also observed, and because encapsulated C_{60} may be lost during ionization, it is difficult to estimate the occupancy of the tetrahedra. The ESI-TOF spectrum of T_2 and C_{60} exhibited similar peaks (Supporting

dx.doi.org/10.1021/ja4083039 | J. Am. Chem. Soc. 2013, 135, 15656−15661

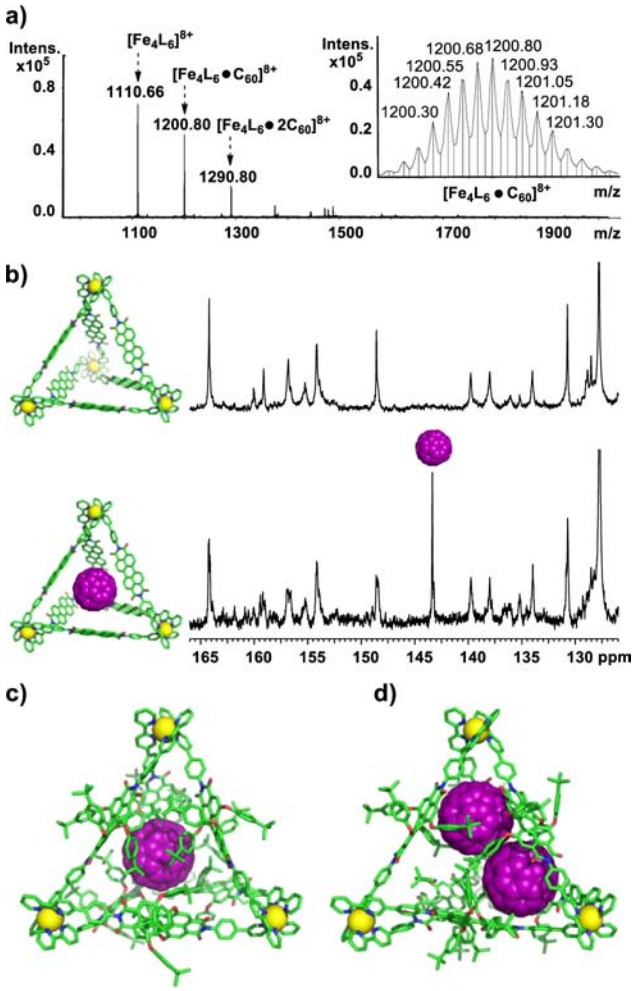

Figure 4. (a) ESI-TOF mass spectrum in CH_3CN of C_{60} encapsulated in $\mathbf{T_1}$. Inset: experimental isotopic distribution for $[Fe_4\mathbf{L}_6{\cdot}C_{60}]^{8+}$. (b) ^{13}C NMR spectra in CD_3CN of $\mathbf{T_2}$ (above) and $\mathbf{T_2}{\cdot}C_{60}$ (below) highlighting the distinct resonance of encapsulated C_{60} at 143.4 ppm. (c) MMFF model of $[Fe_4\mathbf{L}_6{\cdot}C_{60}]^{8+}$. (d) MMFF model of $[Fe_4\mathbf{L}_6{\cdot}2C_{60}]^{8+}$.

Information Figure S14). To further confirm the host–guest encapsulation of C_{60}, a comparison of the ^{13}C NMR spectra of $\mathbf{T_2}$ and $\mathbf{T_2}{\cdot}C_{60}$ in CD_3CN is depicted in Figure 4b. The spectrum of $\mathbf{T_2}{\cdot}C_{60}$ clearly shows an intense extra resonance at 143.4 ppm that corresponds to encapsulated C_{60},[27] confirming the host–guest interaction between C_{60} and $\mathbf{T_2}$ as C_{60} alone is insoluble in CD_3CN.[26]

Encapsulation of C_{60} has a negligible effect on the absorption spectra of $\mathbf{T_2}$. The principle difference upon encapsulation is that $\mathbf{T_2}{\cdot}C_{60}$ shows a higher optical density at 330 nm where C_{60} absorbs (Supporting Information Figure S19). This observation indicates that there is little interaction between the ground states of the host tetrahedron and encapsulated C_{60}, possibly a result of the bulky OPh^{t}Bu bay substituents and the relatively rigid PBI π-surface preventing intimate contact between the PBI core and the convex surface of C_{60}. Because the ground states are relatively unperturbed by encapsulation, subtracting the absorption spectrum of $\mathbf{T_2}$ from the absorption spectrum of $\mathbf{T_2}{\cdot}C_{60}$ yields a difference spectrum that roughly represents the contribution of encapsulated C_{60} to the $\mathbf{T_2}{\cdot}C_{60}$ spectrum. The obtained difference spectrum exhibits λ_{max} = 330 nm, in agreement with the absorption spectrum of C_{60} (λ_{max} = 329 nm). Quantification of the difference spectrum using the molar extinction coefficient of C_{60} gave 1.9 C_{60} guest molecules per host as an estimate of the host–guest occupancy factor (see Supporting Information).

Because the internal volume of the tetrahedron hinges on the orientation of the freely rotating PBI bay substituents, it is difficult to assess the host–guest binding with volume considerations. However, based on the calculated internal volume of $\mathbf{T}_n$ (between 950 and 2150 Å^3) and the volume of C_{60} (597 Å^3), the host–guest occupancies of $[Fe_4\mathbf{L}_6{\cdot}C_{60}]^{8+}$ and $[Fe_4\mathbf{L}_6{\cdot}2C_{60}]^{8+}$ are in good agreement with the empirical 55% rule established by Mecozzi and Rebek for solution-state host–guest encapsulation.[28] Within the tetrahedron, the OPh^{t}Bu bay substituents of the PBI ligands may interact with the guest fullerenes, and by changing orientation, the bay substituents may modulate the internal volume of the host to optimize the host–guest occupancy. In addition, host–guest interactions between the π-surfaces of the OPh^{t}Bu substituents and C_{60} may allow for denser solution-state packing.[29]

Molecular force field MMFF geometry optimizations of singly and doubly occupied host–guest complexes were performed to help visualize the arrangement of C_{60} within the tetrahedron.[22] For $[Fe_4\mathbf{L}_6{\cdot}C_{60}]^{8+}$, C_{60} resides near the center of the capsule, "solvated" by the aromatic OPh^{t}Bu substituents (Figure 4c). This configuration further supports the observed absence of ground-state interactions between host and guest. In the case of $[Fe_4\mathbf{L}_6{\cdot}2C_{60}]^{8+}$, the guest fullerenes are preferentially located closer to the corners of tetrahedral void space, providing sufficient space for both guests (Figure 4d). Future modifications of the bay substituents on the PBI ligand may concurrently enable tuning of the host volume and provide a mechanism for controlled guest uptake and release.[30]

■ CONCLUSIONS

In search of large host molecules that absorb visible light and exhibit redox behavior relevant for host–guest photosensitization, we have designed, isolated, and studied the host–guest chemistry of new metallosupramolecular tetrahedra $\mathbf{T}_n$, composed of photo- and redox-active PBI edges and $[Fe(bpy)_3]^{2+}$ corners. The general $M_4\mathbf{L}_6$ tetrahedral structure was confirmed using a variety of techniques including high-resolution mass spectrometry, DOSY and ^1H NMR spectroscopy, UV–vis spectroscopy, and CV. The dimensions of $\mathbf{T_1}$ and $\mathbf{T_2}$, roughly 3.9 nm across, make these tetrahedra among the largest metallosupramolecular tetrahedra ever reported. Encapsulation of C_{60} was observed and confirmed by ^{13}C NMR spectroscopy, UV–vis spectroscopy, and ESI-TOF mass spectrometry, establishing the tetrahedra as excellent hosts for large guest molecules. Cyclic voltammetry of the visible-light absorbing tetrahedra revealed exceptionally reversible 34 electron cycling between a +18 and a −16 charged species, suggesting that these metallosupramolecular hosts should be suitable to support photo- and electrocatalytic processes. Therefore, our future investigations are focused on the application of these multifunctional tetrahedra as sensitizers for the photo- or electrocatalytic conversion of encapsulated guests.

■ ASSOCIATED CONTENT

Ⓢ Supporting Information

Synthetic details, characterization, NMR spectra, MALDI and ESI-MS, cyclic voltammograms, UV–vis analysis, molecular

dx.doi.org/10.1021/ja4083039 | J. Am. Chem. Soc. 2013, 135, 15656–15661

modeling. This material is available free of charge via the Internet at http://pubs.acs.org.

AUTHOR INFORMATION

Corresponding Author

wuerthner@chemie.uni-wuerzburg.de

Notes

The authors declare no competing financial interest.

ACKNOWLEDGMENTS

K.M. and P.D.F. thank the Alexander von Humboldt Foundation for postdoctoral fellowships. Generous financial support by the DFG (FOR 1806 "Light-induced Dynamics in Molecular Aggregates") and the Bavarian State Ministry of Science, Research, and the Arts for the Collaborative Research Network "Solar Technologies go Hybrid" is gratefully acknowledged.

REFERENCES

(1) Yoshizawa, M.; Klosterman, J. K.; Fujita, M. *Angew. Chem., Int. Ed.* **2009**, *48*, 3418−3438.

(2) (a) Chakrabarty, R.; Mukherjee, P. S.; Stang, P. J. *Chem. Rev.* **2011**, *111*, 6810−6918. (b) Young, N. J.; Hay, B. P. *Chem. Commun.* **2013**, *49*, 1354−1379. (c) Smulders, M. M. J.; Riddell, I. A.; Browne, C.; Nitschke, J. R. *Chem. Soc. Rev.* **2013**, *42*, 1728−1754. (d) De, S.; Mahata, K.; Schmittel, M. *Chem. Soc. Rev.* **2010**, *39*, 1555−1575. (e) Saalfrank, R. W.; Maid, H.; Scheurer, A. *Angew. Chem., Int. Ed.* **2008**, *47*, 8794−8824. (f) Schalley, C. A.; Lützen, A.; Albrecht, M. *Chem.—Eur. J.* **2004**, *10*, 1072−1080.

(3) (a) Laughrey, Z.; Gibb, B. C. *Chem. Soc. Rev.* **2011**, *40*, 363−386. (b) Berryman, B. O.; Dube, H.; Rebek, J., Jr. *Isr. J. Chem.* **2011**, *51*, 700−709. (c) Breiner, B.; Clegg, J. K.; Nitschke, J. R. *Chem. Sci.* **2011**, *2*, 51−56. (d) Fiedler, D.; Leung, D. H.; Bergman, R. G.; Raymond, K. N. *Acc. Chem. Res.* **2005**, *38*, 351−360.

(4) (a) Frischmann, P. D.; Mahata, K.; Würthner, F. *Chem. Soc. Rev.* **2013**, *42*, 1847−1870. (b) Rybtchinski, B.; Wasielewski, M. R. Artificial Photosynthesis for Solar Energy Conversion. In *Fundamentals of Materials for Energy and Environmental Sustainability*; Ginley, D. S., Cahen, D., Eds.; Materials Research Society: Cambridge, UK, 2012; pp 349−364. (c) Puntoriero, F.; Sartorel, A.; Orlandi, M.; La Ganga, G.; Serroni, S.; Bonchio, M.; Scandola, F.; Campagna, S. *Coord. Chem. Rev.* **2011**, *255*, 2594−2601. (d) Flamigni, L.; Collin, J.-P.; Sauvage, J.-P. *Acc. Chem. Res.* **2008**, *41*, 857−871.

(5) Furutani, Y.; Kandori, H.; Kawano, M.; Nakabayashi, K.; Yoshizawa, M.; Fujita, M. *J. Am. Chem. Soc.* **2009**, *131*, 4764−4768.

(6) Murase, T.; Takezawa, H.; Fujita, M. *Chem. Commun.* **2011**, *47*, 10960−10962.

(7) Jagadesan, P.; Mondal, B.; Parthasarathy, A.; Rao, V. J.; Ramamurthy, V. *Org. Lett.* **2013**, *15*, 1326−1329.

(8) (a) Bivaud, S.; Goeb, S.; Croué, V.; Dron, P. I.; Allain, M.; Sallé, M. *J. Am. Chem. Soc.* **2013**, *135*, 10018−10021. (b) Bivaud, S.; Balandier, J.-Y.; Chas, M.; Allain, M.; Goeb, S.; Sallé, M. *J. Am. Chem. Soc.* **2012**, *134*, 11968−11970.

(9) He, C.; Wang, J.; Zhao, L.; Liu, T.; Zhang, J.; Duan, C. *Chem. Commun.* **2013**, *49*, 627−629.

(10) (a) Porel, M.; Chuanng, C.-H.; Burda, C.; Ramamurthy, V. *J. Am. Chem. Soc.* **2012**, *134*, 14718−14721. (b) Bianchini, G.; Scarso, A.; La Sorella, G.; Strukul, G. *Chem. Commun.* **2012**, *48*, 12082−12084. (c) Porel, M.; Jockusch, S.; Parthasarathy, A.; Rao, V. J.; Turro, N. J.; Ramamurthy, V. *Chem. Commun.* **2012**, *48*, 2710−2712. (d) Podkoscielny, D.; Gadde, S.; Kaifer, A. E. *J. Am. Chem. Soc.* **2009**, *131*, 12876−12877.

(11) (a) Würthner, F.; Sautter, A. *Chem. Commun.* **2000**, 445−446. (b) You, C.-C.; Würthner, F. *J. Am. Chem. Soc.* **2003**, *125*, 9716−9725. (c) Sautter, A.; Kaletaş, B. K.; Schmid, D. G.; Dobrawa, R.; Zimine, M.; Jung, G.; van Stokkum, I. H. M.; De Cola, L.; Williams, R. M.; Würthner, F. *J. Am. Chem. Soc.* **2005**, *127*, 6719−6729. (d) Addicott, C.; Oesterling, I.; Yamamoto, T.; Müllen, K.; Stang, P. J. *J. Org. Chem.* **2005**, *70*, 797−801. (e) Stepanenko, V.; Würthner, F. *Small* **2008**, *4*, 2158−2161.

(12) Castellano, F. N. *Dalton Trans.* **2012**, *41*, 8493−8501.

(13) (a) Oliva, A. I.; Ventura, B.; Würthner, F.; Camara-Campos, A.; Hunter, C. A.; Ballester, P.; Flamigni, L. *Dalton Trans.* **2009**, 4023−4037. (b) Haycock, R. A.; Hunter, C. A.; James, D. A.; Michelsen, U.; Sutton, L. R. *Org. Lett.* **2000**, *2*, 2435−2438. (c) Chi, X.; Guerin, A. J.; Haycock, R. A.; Hunter, C. A.; Sarson, L. D. *J. Chem. Soc., Chem. Commun.* **1995**, 2567−2569.

(14) Glasson, C. R. K.; Meehan, G. V.; Motti, C. A.; Clegg, J. K.; Turner, P.; Jensen, P.; Lindoy, L. F. *Dalton Trans.* **2011**, *40*, 10481−10490. (b) Glasson, C. R. K.; Meehan, G. V.; Clegg, J. K.; Lindoy, L. F.; Turner, P.; Duriska, M. B.; Willis, R. *Chem. Commun.* **2008**, 1190−1192.

(15) Lazarte, M.; Marigliano, A. C. G.; Sólimo, H. N. *J. Solution Chem.* **2004**, *33*, 1549−1563.

(16) Osswald, P.; Würthner, F. *J. Am. Chem. Soc.* **2007**, *129*, 14319−14326.

(17) (a) Hristova, Y. R.; Smulders, M. M. J.; Clegg, J. K.; Breiner, B.; Nitschke, J. R. *Chem. Sci.* **2011**, *2*, 638−641. (b) Saalfrank, R. W.; Demleitner, B.; Glaser, H.; Maid, H.; Bathelt, D.; Hampel, F.; Bauer, W.; Teichert, M. *Chem.—Eur. J.* **2002**, *8*, 2679−2683. (c) Caulder, D. L.; Brückner, C.; Powers, R. E.; König, S.; Parac, T. N.; Leary, J. A.; Raymond, K. N. *J. Am. Chem. Soc.* **2001**, *123*, 8923−8938. (d) Beissel, T.; Powers, R. E.; Parac, R. N.; Raymond, K. N. *J. Am. Chem. Soc.* **1999**, *121*, 4200−4206.

(18) (a) Cohen, Y.; Avram, L.; Frish, L. *Angew. Chem., Int. Ed.* **2005**, *44*, 520−554. (b) Megyes, T.; Jude, H.; Grosz, T.; Bako, I.; Radnai, T.; Tarkanyi, G.; Palinkas, G.; Stang, P. J. *J. Am. Chem. Soc.* **2005**, *127*, 10731−10738.

(19) (a) Clark, R. J. H.; Turtle, P. C.; Strommen, D. P.; Streusand, B.; Kincaid, J.; Nakamoto, K. *Inorg. Chem.* **1977**, *16*, 84−89. (b) Krumholz, P. *J. Am. Chem. Soc.* **1953**, *75*, 2163−2166.

(20) Braterman, P. S.; Song, J.-I.; Peacock, R. D. *Inorg. Chem.* **1992**, *31*, 555−559.

(21) Saji, T.; Aoyagui, S. *J. Electroanal. Chem.* **1975**, *58*, 401−410.

(22) *Spartan'08*; Wavefunction, Inc.: Irvine, CA, 2008.

(23) (a) Black, S. P.; Stefankiewicz, A. R.; Smulders, M. M. J.; Sattler, D.; Schalley, C. A.; Nitschke, J. R.; Sanders, J. K. M. *Angew. Chem., Int. Ed.* **2013**, *52*, 5749−5752. (b) Ousaka, N.; Grunder, S.; Castilla, A. M.; Whalley, A. C.; Stoddart, J. F.; Nitschke, J. R. *J. Am. Chem. Soc.* **2012**, *134*, 15528−15537.

(24) Canevet, D.; Pérez, E. M.; Martín, N. *Angew. Chem., Int. Ed.* **2011**, *50*, 9248−9259.

(25) (a) Feng, L.; Rudolf, M.; Wolfrum, S.; Troeger, A.; Slanina, Z.; Akasaka, T.; Nagase, S.; Martín, N.; Ameri, T.; Brabec, C. J.; Guldi, D. M. *J. Am. Chem. Soc.* **2012**, *134*, 12190−12197. (b) Hofmann, C. C.; Lindner, S. M.; Ruppert, M.; Hirsch, A.; Haque, S. A.; Thelakkat, M.; Köhler, J. *J. Phys. Chem. B* **2010**, *114*, 9148−9156. (c) Chamberlain, T. W.; Davies, E. S.; Khlobystov, A. N.; Champness, N. R. *Chem.—Eur. J.* **2011**, *17*, 3759−3767.

(26) Ruoff, R. S.; Tse, D. S.; Malhotra, R.; Lorents, D. C. *J. Phys. Chem.* **1993**, *97*, 3379−3383.

(27) (a) Huerta, E.; Isla, H.; Pérez, E. M.; Bo, C.; Martín, N.; de Mendoza, J. *J. Am. Chem. Soc.* **2010**, *132*, 5351−5353. (b) Suzuki, K.; Takao, K.; Sato, S.; Fujita, M. *J. Am. Chem. Soc.* **2010**, *132*, 2544−2545.

(28) Mecozzi, S.; Rebek, J., Jr. *Chem.—Eur. J.* **1998**, *4*, 1016−1022.

(29) (a) Fairchild, R. M.; Holman, K. T. *J. Am. Chem. Soc.* **2005**, *127*, 16364−16365. (b) Frischmann, P. D.; Facey, G. A.; Ghi, P. Y.; Gallant, A. J.; Bryce, D. L.; Lelj, F.; MacLachlan, M. J. *J. Am. Chem. Soc.* **2010**, *132*, 3893−3908.

(30) (a) Rieth, S.; Hermann, K.; Wang, B.-Y.; Badjić, J. D. *Chem. Soc. Rev.* **2011**, *40*, 1609−1622. (b) Zarra, S.; Smulders, M. M. J.; Lefebvre, Q.; Clegg, J. K.; Nitschke, J. R. *Angew. Chem., Int. Ed.* **2012**, *51*, 6882−6885.